BIOCHEMISTRY
including biophysical chemistry & molecular biology

Article

pubs.acs.org/biochemistry

The Structure and Competitive Substrate Inhibition of Dihydrofolate Reductase from *Enterococcus faecalis* Reveal Restrictions to Cofactor Docking

Christina R. Bourne,*[,†,§] Nancy Wakeham,[†,∥] Nicole Webb,[†,⊥] Baskar Nammalwar,[‡] Richard A. Bunce,[‡] K. Darrell Berlin,[‡] and William W. Barrow[†]

[†]Department of Veterinary Pathobiology, Oklahoma State University, Stillwater, Oklahoma 74078, United States
[‡]Department of Chemistry, Oklahoma State University, Stillwater, Oklahoma 74078, United States

Supporting Information

ABSTRACT: We are addressing bacterial resistance to antibiotics by repurposing a well-established classic antimicrobial target, the dihydrofolate reductase (DHFR) enzyme. In this work, we have focused on *Enterococcus faecalis*, a nosocomial pathogen that frequently harbors antibiotic resistance determinants leading to complicated and difficult-to-treat infections. An inhibitor series with a hydrophobic dihydrophthalazine heterocycle was designed from the antifolate trimethoprim. We have examined the potency of this inhibitor series based on inhibition of DHFR enzyme activity and bacterial growth, including in the presence of the exogenous product analogue folinic acid. The resulting preferences were rationalized using a cocrystal structure of the DHFR from this organism with a propyl-bearing series member (RAB-propyl). In a companion apo structure, we identify four buried waters that act as placeholders for a conserved hydrogen-bonding network to the substrate and indicate an important role in protein stability during catalytic cycling. In these structures, the nicotinamide of the nicotinamide adenine dinucleotide phosphate cofactor is visualized outside of its binding pocket, which is exacerbated by RAB-propyl binding. Finally, homology models of the TMP^R sequences *dfrK* and *dfrF* were constructed. While the *dfrK*-encoded protein shows clear sequence changes that would be detrimental to inhibitor binding, the *dfrF*-encoded protein model suggests the protein would be relatively unstable. These data suggest a utility for anti-DHFR compounds for treating infections arising from *E. faecalis*. They also highlight a role for water in stabilizing the DHFR substrate pocket and for competitive substrate inhibitors that may gain advantages in potency by the perturbation of cofactor dynamics.

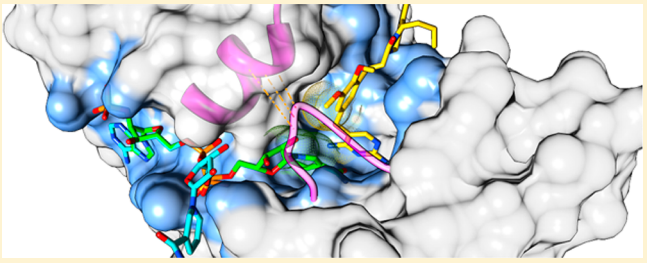

The enzyme dihydrofolate reductase (DHFR) is a critical node within the metabolic pathway for producing folate derivatives that are required for the synthesis of nucleic acids and proteins.[1] There are significant differences in this enzyme that allow specific targeting to prokaryotes, such as with the antibacterial trimethoprim (TMP), in contrast to non-species specific DHFR inhibitors, such as the anticancer drug methotrexate.[2,3] The success of TMP as an antimicrobial is tempered by the prevalence of TMP-resistant (TMP^R) DHFR enzymes, including two forms identified in *Enterococcus faecalis*.[4,5] It is not clear if these TMP^R DHFR sequences are merely maintained as members of larger drug resistance cassettes or if they offer an ecological benefit to the organism.[6] Amino acid changes within TMP^R DHFR enzymes typically impart steric clashes with inhibitors while also negatively impacting the intrinsic catalytic efficiency of the enzyme.[7−9] Our interest in this classic target has been fueled by its favorable properties of "drugability" and selectivity, as well as the growing burden of antimicrobial resistance.[1,10] As such, our long-term goal is the development of anti-folates that can augment or replace TMP and, in so doing, overcome resistance phenotypes.

Increasing resistance to antibacterials has propelled the normal constituent of flora *E. faecalis* to a prominent nosocomial pathogen.[11,12] Given its residence within the gastrointestinal tract of animals, it is likely that the problem of resistance is exacerbated by ingestion of antimicrobial therapies for the treatment of other infections. The most prominent resistance profile is to the antibiotic vancomycin, and the presence of vancomycin resistance in *Enterococci* (VRE) is a harbinger of an expanded resistance profile.[12,13] Current treatments approved by the Food and Drug Administration for simple infections of *E. faecalis* are limited to linezolid, as this organism is intrinsically resistant to the other recommended *Enterococcus* treatment, quinupristin-dalfopristin.[13] More serious and complicated infections, such as *Enterococcus*-mediated endocarditis, do not have a clear regimen of drug therapy but

Received: August 13, 2013
Revised: January 10, 2014
Published: February 4, 2014

dx.doi.org/10.1021/bi401104t | *Biochemistry* 2014, 53, 1228−1238

instead heavily rely on synergistic or additive activities between different classes of antibiotics.

Treatment of *E. faecalis* infections with anti-folates has been controversial because of reports of a reversal of TMP-sulfamethoxazole (SMZ) inhibition by exogenous folinic acid, a DHFR product analogue.[14] The mechanism for this reversal was postulated to be uptake from the surrounding media, thus providing a bypass to the metabolic DHFR node. Although no direct evidence of an entrococcal folate transporter has been documented, a recent study of amino acid uptake by *E. faecalis* through ABC transporters could suggest a role for glutamylation of folate metabolites in their uptake.[15,16] Previous analysis into the impact of folate uptake showed no clear correlation with treatments, and it was concluded that the environment at different sites of infection played a larger role, such as the acidic pH found with urinary tract infections.[17,18] Our studies with *E. faecalis* were initiated as part of a larger investigation of a new series of anti-folate compounds. These anti-folate compounds have previously been demonstrated to be potent inhibitors of *Staphylococcus aureus* in addition to the target organism for their development, *Bacillus anthracis*.[19−21] During experiments to gauge the broad-spectrum capability of this series, it was noted that they were efficacious for *E. faecalis*, including for cases in which a vancomycin resistance (vanB) cassette was present.[19,22]

The DHFR enzyme from *E. faecalis* (Ef DHFR) has an unusual inserted cysteine residue in the binding site, which, on the basis of our initial homology model, was predicted to impact the anti-folate binding. This report reveals the accommodation of this inserted cysteine residue to maintain the binding site structure and also conserved interactions with the anti-folate RAB-propyl as compared to other DHFR enzymes. We have constructed a limited structure−activity relationship for the dihydrophthalazine anti-folate series and found that it closely mirrors that previously derived for *S. aureus* and *B. anthracis*.[20,23] Experiments that aimed to characterize the inhibitory potential in the presence of folinic acid, a stable product analogue, revealed a minimal impact on anti-DHFR inhibitors alone but a modest effect with TMP-SMZ, a synergistic anti-folate mixture that targets DHFR and dihydropteroate synthetase (an enzyme upstream from DHFR). The crystallized Ef DHFR reveals two conformations for the ribose−nicotinamide portion of the NADPH cofactor, which is further exacerbated by the RAB-propyl anti-folate. Finally, we have constructed homology models for the DHFR enzymes reported to impart TMP resistance to *E. faecalis* strains. One of these mutated DHFR enzymes, encoded by the *dfrK* gene, contains amino acid substitutions that are predicted to block TMP and RAB-propyl binding. The other mutated DHFR enzyme is encoded by the *dfrF* gene and has widely distributed changes in sequence that are expected to impact the global stability and cofactor interactions of this protein.

EXPERIMENTAL PROCEDURES

Methods for the synthesis, purification, and verification of the composition of racemic dihydrophthalazine compounds used in this work have been published previously.[24]

Methods for broth microdilution minimal inhibitory concentration (MIC) determinations closely followed the guidelines put forth by the Clinical Laboratory and Standards Institute as well as previous citations.[19,25] The bacterial species tested were *E. faecalis* strain ATCC 29212 and *S. aureus* strain ATCC 29213. For evaluation of media, aliquots of CAMHB growth media were titrated with hydrochloric acid to a pH value of 5.5−6.0, or folinic acid was added to a concentration of 0.1 μg/mL, as in previous reports.[14] The MIC value is reported as the lowest tested concentration of a compound that prevents growth either visible to the eye or detectable by turbidity measured at 600 nm.

Enzymatic assays were performed in a 96-well format as described previously in detail.[19] The assay employed purified recombinant C-terminally StrepII-tagged *E. faecalis* DHFR protein at a final concentration of 2.5 μg/mL and yielded an activity of ∼1.5 nmol of dihydrofolate reduced/min. Reduction of dihydrofolate to tetrahydrofolate was monitored by following the change in absorbance of a redox-sensitive dye [3-(5-dimethylthiazol-2-yl)-5-(3-carboxymethoxyphenyl)-2-(4-sulfophenyl)-2*H*-tetrazolium (MTS) (Promega)] at a wavelength of 450 nm. The concentration of the compound resulting in 50% absolute inhibition was calculated with a four-parameter curve fit within the plate reader software KC Jr.[26] This value was used in combination with an experimentally determined K_m value of 10.9 ± 0.8 μM for the dihydrofolate substrate to derive the K_i for each inhibitor, as calculated by the Cheng−Prusoff formalism.[27]

The gene for Ef DHFR was cloned from genomic material extracted from vancomycin-resistant *E. faecalis* strain ATCC 700802. Primer sequences introduced a TEV cleavage site at the N-termini and a thrombin cleavage site at the C-termini of the protein coding sequence. Protein was expressed from the pPSG-IBA3 vector (IBA Lifesciences) in *Escherichia coli* strain BL21(DE3)pLysS (Invitrogen) grown in Terrific Broth and induced for 20 h using 1 mM IPTG at 20 °C. Cultures were lysed using BugBuster (EMD Millipore) supplemented with benzonase (EMD Millipore), a reducing agent, and the protein inhibitor cocktail, and the clarified lysate was applied directly to a prepacked column of Strep-Tactin Superflow (IBA Lifesciences). The eluted protein was >95% pure as determined by sodium dodecyl sulfate−polyacrylamide gel electrophoresis analysis and, after buffer exchange and protein concentration, was used directly for enzymatic assays. Preliminary experiments determined the C-terminal Strep tag did not affect enzyme activity or inhibition by RAB-propyl (data not shown).

For crystallization, NADPH was added at equimolar concentrations, and the affinity tag was removed by cleavage with thrombin (EMD Millipore) following the manufacturer's recommendations. The sample was again run over the Strep-Tactin resin, and the cleaved protein was chromatographed over a Sephycryl-100 column (GE Lifesciences). The RAB-propyl inhibitor was added to saturation in the protein sample, incubated for 3 h at room temperature, and centrifuged for 10 min prior to the initiation of the crystallization trials. Crystallization was successful using 96-well sitting-drop vapor diffusion plates containing 150 μL of a well solution and mixed in equal 0.8 μL volumes with protein at 16.5 mg/mL in 20 mM Tris (pH 8), 150 mM NaCl, and 2 mM DTT. Crystals of Ef DHFR grew from a well containing 5% polyethylene glycol 3350 and 1.5 M ammonium citrate dibasic (pH 7) and appeared within 1 week at room temperature. Crystals complexed with RAB-propyl were grown from 1.1 M ammonium tartrate dibasic (pH 7) at 4 °C and required between 2 and 3 months to appear. The uncleaved TEV site remained intact and was found to participate in crystal packing interactions.

X-ray data were collected at 100 K using a Rigaku generator and captured on an RaxisIV^{++} image plate. Data were indexed

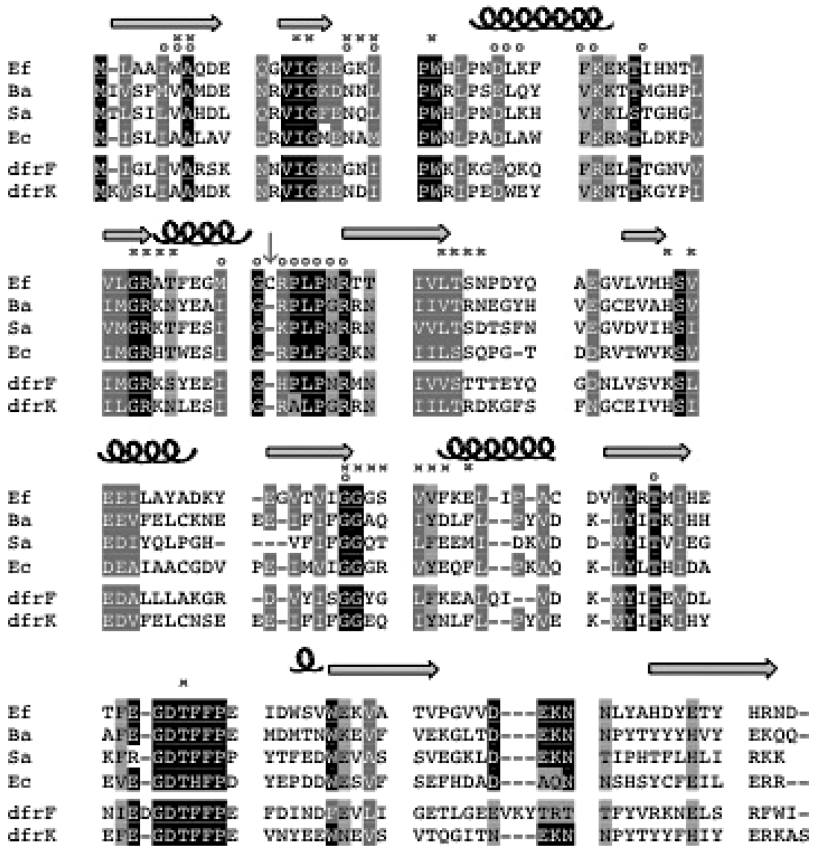

Figure 1. Amino acid sequence alignment for DHFR enzymes from *E. faecalis* (Ef), *B. anthracis* (Ba), *S. aureus* (Sa), and *Es. coli* (Ec). Residues contacting the RAB-propyl inhibitor in Ef DHFR are noted with a circle, and those contacting the NADPH cofactor are noted with a times sign. The inserted cysteine residue in Ef DHFR is indicated with an arrow; secondary structure is also indicated. Completely conserved residues are highlighted in black boxes; conservative changes in sequence are highlighted in dark gray, and weakly conserved residues are highlighted in light gray.

with iMosflm[28] and scaled with Scala.[29] Molecular replacement was conducted using Phaser[30] as incorporated into the Phenix software suite.[31] The model for molecular replacement was a DHFR structure from *Bacillus stearothermophilus* [Protein Data Bank (PDB) entry 1ZDR],[32] which was the model selected as most similar in sequence from homology modeling studies (below). Refinement was conducted with Phenix, and manual model adjustments were made with Coot.[31,33] Analysis of atomic contacts was aided by the Ligand Protein Contacts server;[34] diagrams of contacts were made with Ligplot+.[35] Refined models and structure factor data have been deposited in PDB (4M7U and 4M7V).

Homology models were constructed with the SwissModel automated pipeline.[36] For both of the TMP-resistant sequences, the template with most similar sequence was the DHFR from *B. anthracis*. For the *dfrF* model, the template was the structure in PDB entry 4ELG, which is 35% identical (61.2% strongly conserved) and coincidentally was cocrystallized with a related dihydrophthalazine.[9] For the *dfrK* model, the template selected by the automated procedure was from PDB entry 3S9U, which is 65% identical (87.9% strongly conserved) in sequence.[37] RAB-propyl was manually docked into the site based on superposition with Ef DHFR, and the resulting models were subjected to geometry minimization using Phenix.[31]

RESULTS AND DISCUSSION

Sequence Characteristics of *E. faecalis* Dihydrofolate Reductase Enzymes. The overall sequence of the *E. faecalis* (Ef) DHFR protein maintains the identity of residues known to contact the dihydrofolate substrate or inhibitor (Figure 1, circles) and the nicotinamide adenine dinucleotide phosphate (NADPH) cofactor (Figure 1, crosses), as well as a catalytic aspartic acid (Ef residue 27).[19,23,38] Positions previously shown to mediate the TMP^R phenotype in *B. anthracis* and *S. aureus* encode the susceptible variants in Ef DHFR: Ile96 and Val102.[7,8] A dynamic catalytic cycle has previously been mapped using structures of *Es. coli* DHFR.[38] This indicated a role for nicotinamide mobility coordinated to the Met20 loop, comprising Ef residues 13−25. The most notable amino acid change for the Ef DHFR in this region is an Asn to Gly mutation at position 18. Of note, the human DHFR possesses a double-proline insertion at the equivalent position, which is known to limit movements of the loop during catalysis that, only in concert with other mutations in the *p*-aminobenzoyl glutamate (pABG) binding cleft (see below), improves the catalytic efficiency.[39] Throughout the catalytic cycle, this loop movement in bacterial DHFR occurs in concert with other structural variations around the substrate binding site, particularly in the pABG cleft spanning residues 50−58 in Figure 1. A particularly unusual sequence change identified for the Ef DHFR is the insertion of a cysteine residue at position 52 (Figure 1, arrow). This correlates with the "PEKN" insertion found in human DHFR, which serves as a lid over the substrate

dx.doi.org/10.1021/bi401104t | *Biochemistry* 2014, 53, 1228−1238

DHF site and is a major determinant blocking interaction of the current anti-folate series with human DHFR.[23,39]

The first TMP^R DHFR enzyme identified in *E. faecalis* is the *dfrF* sequence (Figure 1); it was found only in select strains and is harbored chromosomally but within a transposon cassette.[4] Amino acids at positions known to mediate TMP^R are not present, and a susceptible phenotype is predicted on the basis of these sequence data.[7,8] However, previous studies with compounds related to the current series clearly demonstrated *dfrF*-mediated resistance.[22] The *dfrK* gene encodes the other TMP^R DHFR enzyme identified in *E. faecalis*. It was identified within a *tetL* resistance cassette located chromosomally in a transposon-mediated mobile genetic element and is believed to have originated in a staphylococcal species.[5] Its resistance phenotype is likely correlated with a Tyr at position 102, as this has been demonstrated to invoke TMP^R in *B. anthracis* and *S. aureus* (Figure 1).[7,8] In addition, it has a mutation of a weakly conserved Leu residue at position 28 to encode a much larger Trp, and this is visualized to protrude into the binding pocket (see below and Figure S1 of the Supporting Information).

Efficacy of Trimethoprim-Based Dihydrophthalazine Inhibitors. The inhibitor series used in these studies maintains a scaffold based on the structure of TMP, containing a 2,4-diaminopyrimidine ring and a central dimethoxyphenyl ring. The current inhibitor series is extended beyond this scaffold to include a dihydrophthalazine heterocycle with variations appended at a chiral center on the pyridazine ring. A collection of these racemic inhibitors has been screened (Table 1) with the organism *E. faecalis* to assess growth inhibition, presented as the minimal inhibitory concentration (MIC, in micrograms per milliliter), and for competitive inhibition of the purified DHFR enzyme (K_i, in nanomolar).

Table 1. Efficacy of TMP and Dihydrophthalazine Series of Compounds with *E. faecalis* 29212

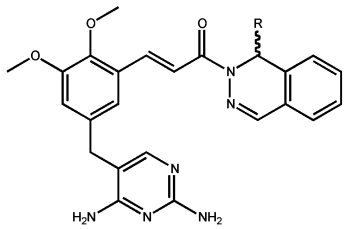

	modification (R)	MIC (μg/mL)	K_i (nM) (SEM)
TMP		0.06−0.125	2.1 (0.2)
RAB	propyl	0.06−0.125	4.5 (0.1)
OSU31	isopropyl	0.03−0.06	3.8 (0.1)
OSU35	trifluoropropyl	0.03−0.125	3.8 (0.1)
OSU52	isobutyl	0.125	3.5 (0.2)
OSU53	isobutenyl	0.06−0.125	3.8 (0.2)
OSU69	1-ethylpropyl	0.5	7.4 (0.1)
OSU34	phenyl	0.06−0.125	2.6 (0.2)
OSU77	*m*-fluorophenyl	0.125	4.8 (0.3)
OSU45	*p*-fluorophenyl	0.125	5.6 (0.2)
OSU15	cyclohexyl	0.25−0.5	2.7 (0.2)
OSU37	*p*-methylphenyl	0.25	5.1 (0.3)
OSU66	*m*,*m*′-dimethylphenyl	0.25−0.5	7.1 (0.1)
OSU79	*o*-methylphenyl	0.125	7.2 (0.2)
OSU60	benzyl	0.5	5.0 (0.1)
OSU67	*p*-methylbenzyl	0.5−1.0	6.2 (0.2)
OSU72	*p*-methoxybenzyl	4−8	6.7 (0.2)
OSU75	*p*-trifluoromethoxybenzyl	1.0	18.8 (0.1)

These values were assessed relative to those for TMP, which has a MIC of 0.06−0.125 μg/mL and a K_i of 2.1 nM. The compound in the crystal structure, RAB-propyl, is the founding member of this inhibitor series and has an MIC equivalent to that for TMP. Appending fluorine atoms to the termini of the propyl moiety modestly improved it MIC to 0.03−0.125 (OSU35), but with a clear improvement in the K_i value (4.5 nM for the propyl compound RAB vs 3.8 nM for the trifluoropropyl compound OSU35). In contrast, including fluorine atoms on the phenyl moiety of OSU34 decreased the efficacy, as seen for compounds OSU77 (*m*-fluorophenyl) and OSU45 (*p*-fluorophenyl) (Table 1). Smaller linear or branched alkyl chains are well-tolerated, with K_i values in the range of 3.5−4.5 nM, with the value of OSU69 (1-ethylpropyl) representing an upper limit at 7.4 nM, while and all others tested had values clustered closely around 3.8 nM (Table 1). Compound OSU15 (cyclohexyl) is unique among this collection as it is the only saturated ring, and while it has among the best K_i values at 2.7 nM, it has some of the poorer MIC values (0.25−0.5 μg/mL). Finally, as the moieties become larger and more complex, there is a compensatory loss of activity, as noted for compounds OSU37 (*p*-methylphenyl), OSU66 (*m*,*m*′-dimethylphenyl), and OSU79 (*o*-methylphenyl), all with K_i values of >5.0 nM. This is made worse for even larger compounds such as OSU60 (benzyl), OSU67 (*p*-methylbenzyl), OSU72 (*p*-methoxybenzyl), and OSU75 (*p*-trifluoromethoxybenzyl).

To address previous observations of increased MIC values for *E. faecalis* with anti-folates and in the presence of folinic acid, the MIC assay was performed with compounds RAB-propyl, OSU34 and OSU53, TMP, and TMP-SMZ at acidic pH and with the addition of exogenous folinic acid.[14] These results clarify a significant role for an acidic environment with both *E. faecalis* and *S. aureus*, which caused an increase in MIC of 2−3-fold for TMP or TMP-SMZ and of 1−2-fold for the current anti-folates (Table 2). Exogenous folinic acid, which can be metabolized by enzymes downstream from DHFR, can presumably exert an effect only if it is taken up from the surrounding media. In experiments with *S. aureus*, no change in MIC was noted, while with *E. faecalis*, shifts in MIC of up to 1-fold were noted with TMP and the current anti-folates (Table 2). Interestingly, the major effect of folinic acid in the media was an increase in the MIC value for TMP-SMZ by 2−3-fold, and this was specifically with *E. faecalis*.

Ef DHFR Structure and RAB-propyl Binding. To fully characterize the binding interactions between RAB-propyl and Ef DHFR, and particularly any role for the inserted cysteine residue at the active site, we completed the crystal structures of the Ef DHFR enzyme with NADPH and with RAB-propyl to 2.3 Å, or without RAB-propyl to 2.1 Å (Table 3). These structures refined to acceptable *R* factor values, and the models satisfy criteria for geometry and protein packing. Among the noted crystal packing interactions, the N-terminal TEV site remained uncleaved and participated in packing against a symmetry-related molecule in both structures, although the orientation of this segment was different in the absence and presence of RAB.

These structures have revealed that, in contrast to the homology model, the inserted Cys residue is folded back onto the surface of the protein, pulling this loop away from the pocket relative to other DHFR enzyme structures (Figure

dx.doi.org/10.1021/bi401104t | *Biochemistry* 2014, 53, 1228−1238

Table 2. Effect of Acidic pH and Exogenous Folinic Acid on MIC Values for Anti-Folates and Control Compounds

	MIC (μg/mL)					
	E. faecalis 29212			*S. aureus* 29213		
	pH 5.8	pH 7	folinic acid	pH 5.8	pH 7	folinic acid
TMP	1.0	0.125−0.25	0.25−0.5	8	2	2−4
TMP-SMZ	0.06−0.125	≤0.03	0.25	0.125−0.25	0.125	0.125
RAB	0.125−0.25	0.06	0.06−0.125	0.25	0.03−0.06	0.06
53-isobutenyl	0.25	0.06−0.125	0.125−0.25	0.25−2	0.06−0.125	0.125
34-phenyl	0.25	0.06−0.125	0.125−0.25	0.5	0.125−0.25	0.125
VAN	1−2	1−2	2−4	1	1	1
DOX	2	4	4	0.125−0.25	0.25	0.25

Table 3. Crystallographic Data for *E. faecalis* DHFR

	with NADPH	with NADPH and RAB-propyl
PDB entry	4M7U	4M7V
space group	$P4_12_12$	$P4_12_12$
cell dimensions (Å)	63.25 ($a = b$), 97.15	63.25 ($a = b$), 97.15
resolution (Å) (highest shell)	52.8−2.10 (2.18−2.10)	53−2.3 (2.38−2.30)
	Data Collection	
R_{sym}	9.7 (39.4)	4.1 (18.4)
$I/\sigma I$	9.0 (3.4)	17.4 (6.0)
completeness (%)	98.2 (89.7)	99.4 (100)
redundancy	4.5 (4.4)	4.2 (4.2)
mosaicity	0.33	0.43
Wilson *B* factor (Å^2)	26.5	35.7
	Refinement	
resolution (Å)	40.6−2.10	40.6−2.30
no. of reflections	11737 (1064)	9220 (903)
R_{work}/R_{free}	18.6/22.3	19.0/26.5
no. of atoms		
protein	1363	1334
ligand/ion	96	163
water	131	63
B factor		
protein	22.7	30.3
ligand/ion	21.6 (NADPH)	29.5 (RAB)
		25.4 (NADPH)
water	28.6	33.1
root-mean-square deviation		
bond lengths (Å)	0.008	0.008
bond angles (deg)	1.23	1.22
Ramachandran (%)		
favored	98	97
outliers	0	0
Clashscore	10.6	11.2

2A,E,F). This is in contrast to the homology model that, based on a template from a *Bacillus* species, placed the cysteine residue as impinging on the edge of the substrate binding site and partially occluding the opening (Figure 2E). As we have noted for *B. anthracis*, an arginine at position 53 extends over the site and has a role in enantiomer selection of RAB-propyl and related anti-folates. The homology model of Ef DHFR maintained this and, when the binding site was empty, was predicted to protrude into the site. As seen in the structure of Ef DHFR with RAB-propyl (Figure 2A,E), the Arg53 residue is projected up and out of the site, in concert with placing Cys52 at the edge of the binding pocket, and further back on the protein domain. The cysteine residue does not participate in a disulfide bond within the structure. It is, however, related by crystal symmetry to Cys52 of another molecule with an approach of sulfur atoms at 6.9 Å.

The loop placement as a result of the inserted residue also causes a movement of the helix preceding this loop of up to 0.6 Å, which has a large impact on NADPH binding (see below). Surrounding residues in this loop are also pulled away, resulting in a widening of the Ef DHFR binding site as compared to other bacterial DHFR enzymes (Figure 2E). This structure revealed the RAB-propyl inhibitor situated in the substrate pocket with a placement conforming to a known hydrogen bonding network to the 2,4-diaminopyrimidine ring, a relatively hydrophobic groove to support the central dimethoxyphenyl ring, and a hydrophobic cavity to accommodate the dihydrophthalazine moiety (Figure 2A,C). For either position, only the *S*-enantiomer of the propyl modification is visible in the electron density (Figure 2A,B).

The phthalazine moiety adopts two mutually exclusive conformations within the binding site with a more deeply buried position in approximately two-thirds of the molecules within the crystal lattice (Figure 2A, yellow). The second position is achieved by torsion around the acryloyl linker, which displaces the dihydrophthalazine moiety at an angle of ∼40° and results in a displacement of 2.8−4.7 Å at the dihydrophthalazine heterocycle (Figure 2A, cyan). The second position places the dihydrophthalazine in a more solvent-exposed position adjacent to a cavity created above Leu63 and the loop containing inserted Cys52. The positioning of the more solvent-exposed RAB-propyl results in a loss of hydrophobic interactions with Pro64, Arg66, and Ala40, reflected in a loss of ∼10% of the buried surface area of RAB-propyl in the complex (total surface area of ∼790 Å^2). The alternate position of the dihydrophthalazine translates along the RAB-propyl molecule and shifts the central ring position ∼0.6 Å closer to the NADPH site (Figure 2A, inset). The closest approach of either RAB-propyl conformation to the NADPH cofactor is 3.2 Å, but the more deeply buried RAB-propyl buries 40.9 Å^2 of surface area with NADPH as compared to the more solvent-exposed version, which buries 63.7 Å^2 of surface area with NADPH due to the translated position.

The floor of the binding pocket in the Ef DHFR binding site is not as deep as in other bacterial DHFR enzymes because of a Phe at position 31 rather than a Val or a smaller hydrophobic residue (Figure 1).[19,23] This places the face of the dihydrophthalazine moiety directly adjacent to the side chain of Leu55. The proximity to Leu55 is consistent with both the observed orientations and is positioned to result in steric repulsion of the *R*-enantiomer in the more buried phthalazine

dx.doi.org/10.1021/bi401104t | *Biochemistry* 2014, 53, 1228−1238

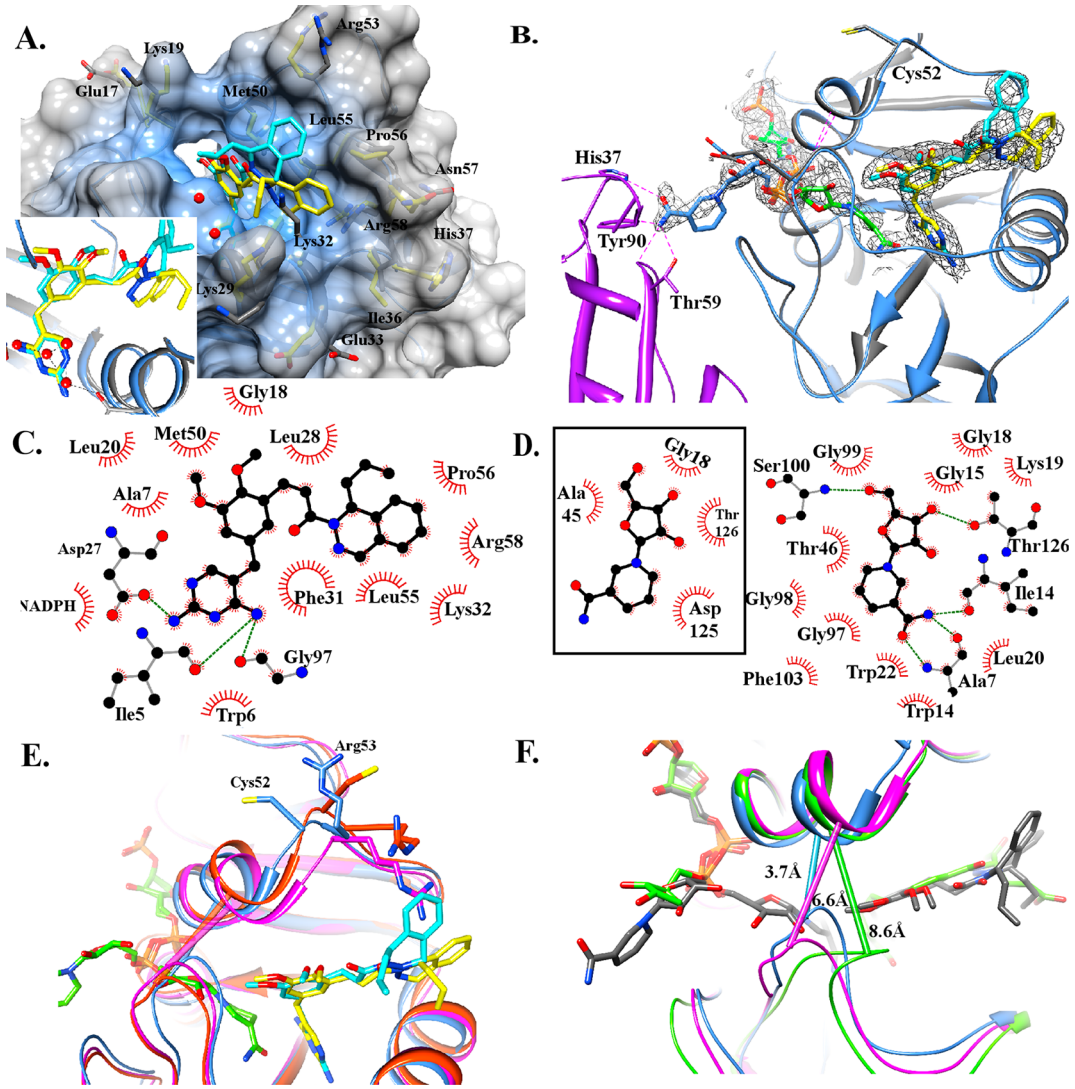

Figure 2. Details of the Ef DHFR binding site and interactions with the inhibitor RAB-propyl. (A) The two positions for the phthalazine of RAB-propyl (yellow and cyan) are visualized in the cocrystal structure. Two water molecules (red spheres) are seen at the periphery of the binding site, by the termini of the propyl moiety. In the inset, four ordered water molecules (red spheres) are seen buried in the substrate binding site in the absence of inhibitors or substrate. (B) The cocrystal structure (blue backbone) is superposed with the structure of Ef DHFR with an empty substrate binding site (gray backbone); the inserted residue Cys52 is shown. Electron density ($2F_o - F_c$ coefficients with structure factors from an initial molecular replacement solution not containing ligands, and contoured at 0.8σ) is shown for RAB-propyl and the NADPH cofactor, which both occupy alternate positions. The externally bound nicotinamide is oriented to interact with the indicated residues from a symmetry-related molecule (purple). (C) Two-dimensional representation of the binding interactions between RAB-propyl and Ef DHFR. Hydrogen bonds are depicted as green dashes, and hydrophobic interactions are depicted by red hatched semicircles. Note that the hydrophobic contacts with Pro56, Arg58, and Lys32 are lost in the second position (colored cyan in panel A). (D) Two-dimensional representation of the binding interactions between the ribose−nicotinamide component of the NADPH cofactor and the Ef DHFR. Hydrogen bonds are depicted as green dashes, and hydrophobic interactions are depicted by red hatched semicircles. The inset shows a two-dimensional representation of the interactions between the externally bound nicotinamide and the Ef DHFR protein. There are no hydrogen bonds in this orientation of the nicotinamide. (E) Superposition of the Ef DHFR cocrystal structure (blue), including the two RAB-propyl positions in the substrate site (yellow and cyan), with the homology model of Ef DHFR (orange) and the DHFR enzyme from *B. anthracis* (magenta). The position of the inserted residue Cys52 is shown for both the experimentally determined (blue) and modeled (orange) structures, as is Arg53 for all three structures. (F) The cocrystal structure of Ef DHFR (blue) with RAB-propyl (gray) is superposed with two conformations of *Es. coli* DHFR, one with an "occluded" Met20 loop and empty substrate pocket (PDB entry 1RX1, magenta) and one with a "closed" Met20 loop and folinic acid in the substrate pocket (PDB entry 1RX6, green). Distances denote the width of the cleft through which the nicotinamide moiety of NADPH accesses the catalytic pocket.

position (Figure 2A,C). For the more solvent-exposed dihydrophthalazine position, there is no obvious deterrent within the binding site to the placement of an *R*-enantiomer, despite an adjacent indentation that appears to be suitable at the Cys52-containing loop. It is of note that Arg53 appeared to sterically block docking of the *R*-enantiomer in previous structures, while in Ef DHFR, the Arg53 residue is folded back on the surface (Figure 2A,E). A final notable feature is an accessible surface depression on the opposite side of the binding site, and in line with the propyl group, which could allow larger or planar modifications to interact favorably with Leu28 (Figure 2A). This region can also interact favorably with polar groups, and in the +RAB-propyl structure, two water molecules are ordered in this pocket. They are coordinated by

dx.doi.org/10.1021/bi401104t | *Biochemistry* 2014, 53, 1228−1238

His23 and Lys29, as this is the likely interaction with the more efficacious OSU35 (trifluoropropyl) compound versus RAB-propyl.

Changes in Ef DHFR Structure upon Binding of RAB-propyl. The ability to compare the NADPH-complexed structure with and without the RAB-propyl inhibitor offers insight into the consequences of binding on protein conformation and on the ordered waters. In the absence of RAB-propyl, four water molecules are seen deep within the pocket (Figure 2A, inset). Two of these are positioned at the location occupied by the diamino groups of the pyrimidine ring, which correspond to diamino groups found on the substrate pterin ring. These diamino moieties, and the requisite hydrogen bonds formed between them, or between the observed water molecules, with conserved protein atoms, are known to be major determinants of binding in the substrate pocket.[40] The third buried water molecule is at a position corresponding to the face of the pyrimidine ring when bound, and the fourth buried water is at a position adjacent to the pyrimidine ring binding site. The latter two water molecules provide additional binding partners for the first two waters, which appear to serve as direct placeholders for the substrate.

Upon complexation of RAB-propyl, the main chains of the protein on each side of the substrate binding pocket are closer together. Residues 26−34 encode a helix, and once RAB-propyl binds, this helix more closely approaches another helix encoded by residues 45−50 that is present on the opposing side of the binding site. This change is seen to compress the width of the overall shape of the binding site. Another change in the overall shape is a lengthening of the binding site cavity. This change results from movement of residues 32−36, located below the dihydrophthalazine, and residues 56−58, located at the periphery of the dihydrophthalazine moiety (Figures 1 and 2A,B). Movement of side chains is also noted, as Lys29 moves inward toward the propyl-occupied space in the complex and Lys32 moves outward and becomes disordered, leading to compensatory movement of Glu33. Arg58 is shifted to permit the dihydrophthalazine access to the site and causes His37 to move away from the site as well as a variation of the rotomer for Ile36. In addition, Met50 must turn slightly to accommodate the planar central aromatic ring of RAB-propyl. While there are other minor adjustments in the binding site resulting from RAB-propyl complexation, the inserted cysteine residue shows absolutely no change in position (Figure 2B).

Alternate Conformation of the NADPH Cofactor. Regardless of the presence of RAB-propyl, the nicotinamide−ribose moiety of the NADPH cofactor presents a well-ordered second conformation protruding from the surface of the protein and into the solvent (Figure 2B). This orientation is achieved by rotation around the phosphate−sugar linkage of the nucleotide moiety, as was noted in early studies with *Es. coli* DHFR structures.[38] This rotation places the ribose sugar and nicotinamide groups outside the protein pocket, and the nicotinamide engages in long-range crystal packing with residues His37 (3.7 Å), Thr59 (3.75 Å), and Tyr90 (4.4 Å) of a symmetry-related molecule (Figure 2B). This exposed position lacks interactions observed between the buried NADPH conformation and the protein, including five hydrogen bonds formed with residues Ala7, Ile14, Ser100, and Thr126. Further, hydrophobic interactions with Trp14, Gly15, Leu20, Trp22, Gly97, Gly98, and Phe103 are lost (Figure 2B,D). Crystallographic refinement of occupancies of these two mutually exclusive NADPH conformations indicates a preference of ∼60% for the externally bound form. This is exacerbated by the presence of RAB-propyl, in which the level of the externally bound form is increased to ∼80%. The limited 20% occupancy within the pocket when RAB-propyl is also present is visualized as discontinuous electron density at the nicotinamide moiety (Figure 2B).

The point of divergence in the NADPH orientation is centered on residue Gly18, which, in bacterial DHFR enzymes, is typically a larger and polar Asn residue (Figure 1). It is located at the apex of a previously identified flexible loop in *Es. coli* (the "Met20" loop).[38] Upon comparison to structures of DHFR from *Es. coli*, *S. aureus*, and *B. anthracis*, it is apparent that the insertion of Cys52 induces the helix immediately upstream, which faces the NADPH site, to shift into the NADPH site (Figure 2E,F). This results in less space between the two lobes of the protein that comprise a channel for nicotinamide access. As a means of quantifying this closure of the nicotinamide channel in Ef DHFR, distances were measured spanning the α-carbons of residues Ef Gly18, found in the loop, and Ef Gly49, the closest residue in the helix across from this loop (Figure 2F). For Ef DHFR, this results in only 3.7 Å of available space between the α-carbon atoms of the opposing residues. In contrast, *Es. coli* DHFR displayed an "occluded" loop conformation in which this opening ranges from 5.9 Å (PDB entry 1RX1) to 6.6 Å (PDB entry 1RX9), and up to 8.6 Å in the "closed" loop form seen with the product analogue (PDB entry 1RX6), as measured from Asn10 to Ser49 in each instance.[38] For *B. anthracis* DHFR (from Asn19 to Ala50, PDB entry 3FL8) or *S. aureus* DHFR (from Asn18 to Ser49, PDB entry 3M08), upon formation of a complex with RAB-propyl, this distance is 6.0 Å.[19,23] The net result is reduced access to the nicotinamide pocket in the Ef DHFR, which may explain the favored alternate conformation external to the catalytic site.

The structural effect of the insertion at position 52 is a movement of the loop, which also shifts the preceding helix that lines the opening to the NADPH site. This helix protrudes farther into the cofactor site, which results in a narrowing of the cleft by which the nicotinamide−ribose moiety accesses the catalytic portion of the binding site. In *Es. coli* DHFR, this Met20 loop was identified in crystal structures to form an open, occluded, and closed structure.[38] The configuration of the equivalent loop in Ef DHFR most closely aligns with the occluded form, which for *Es. coli* was attained by including an oxidized NADPH and an empty substrate pocket (i.e., PDB entry 1RX9).[38] In the series of *Es. coli* structures, the nicotinamide−ribose moiety was also forced into the externally bound form when the substrate site was filled with a product analogue (i.e., PDB entry 1RX6). However, in the latter case, the loop in question collapsed into the closed form, which is more deeply embedded than that seen in Ef DHFR. These observations provided the rationale for linking the movements to binding and to release as distinct parts of the catalytic cycle. Similarly, other studies were able to purposefully displace the nicotinamide−ribose moiety through inhibitor binding in the DHFR enzyme from the fungal organism *Candida albicans*.[41] In each previous case of an externally bound NADPH conformation, there was disorder that prevented clear interpretation beyond the ribose unit. In the current structures of Ef DHFR, the involvement in crystal packing has allowed very clear visualization of density for the external nicotinamide, and in addition, the preceding ribose sugars of the current

structures and the previous *Es. coli* and *C. albicans* structures superpose well.

It is unlikely that the crystallization forces could remove the nicotinamide from its buried position within the pocket, particularly as the packing contacts that are formed are fewer in number and display longer bond distances. This leads us to conclude that this external conformation of the nicotinamide must exist within the solution and that the crystallization process is selecting from this population. We also note that, over the time course of crystallization, the NADPH is likely oxidized to $NADP^+$ and this oxidation, yielding a planar conformation for the nicotinamide, would facilitate liberation of the nicotinamide from within the catalytic pocket.[38,42] For the structure without RAB-propyl, the electron density for the nicotinamide within the pocket clearly indicates a puckered conformation, supporting a reduced form; however, in the structure with RAB-propyl, the electron density is too diffuse to distinguish the ring conformation. In either structure, the externally bound nicotinamide could be modeled as either planar or puckered and still satisfy the electron density, such that one can hypothesize it is a mixture of oxidized and reduced forms. Our data demonstrate that the nicotinamide pocket within the protein is less accessible, resulting in a higher proportion of externally located forms regardless of the nicotinamide oxidation state, which are then available for interactions within the crystal lattice.

Trimethoprim-Resistant DHFR Enzymes in *E. faecalis* Strains. The original description of the DHFR enzyme sequence from *E. faecalis* also revealed a second integrated DHFR gene in a subset of strains that displayed elevated MIC values for TMP; as such, this was evidence of a TMP^R DHFR enzyme and was named *dfrF*.[4] We have constructed a homology model to identify amino acid changes that could mediate this resistance to TMP and, in addition, show what impact they would have on RAB-propyl or similar anti-folate binding. Typical residues imparting resistance to TMP are not present in the sequence, such as a Phe (TMP^S) to Tyr (TMP^R) mutation at position 102 (Figure 1). Visual inspection of the model also did not reveal any notable obstruction to RAB-propyl or anti-folates within the binding site.

However, the resulting model for the *dfrF*-encoded protein scored poorly with regard to estimations of quality, as might be expected because of the low level of sequence identity (35%) and sequence conservation (61.2%) with the most closely matching template.[43] The resulting QMEAN score of 0.725 indicates that the modeling parameters were successful, based on a scale of 0−1, with 1 being the most ideal.[44] The QMEAN *Z* score estimates the "nativeness" of the internal protein packing in comparison to crystallographically determined structures, and in this measure, the *dfrF*-encoded model scored very poorly (−0.796).[44] Visual examination of the minimized homology model highlighted instances of unpaired, buried polar residues as well as residues that impede on the NADPH site access, particularly Glu49. Other disruptions to packing within the NADPH site were noted, such as Tyr97, which would provide a steric clash with the first phosphate of the NADPH. Finally, this molecule has lost a $\pi-\pi$ stacking interaction between residue Tyr 30, which in the *dfrF* sequence is a Gln, and residue Phe 159, which in the *dfrF* sequence is an Arg. This is likely due to an insertion of three residues (Val-Lys-Tyr) immediately upstream of the Arg residue, which alters the register of the model (Figure S1 of the Supporting Information).

We also constructed a homology model for the *dfrK*-encoded protein, the other TMP^R DHFR identified to date in select strains of *E. faecalis*.[5] This model is based on a template that has a sequence that is 64.2% identical (87.9% strongly conserved), and indicators of model quality were favorable (QMEAN score of 0.806, QMEAN *Z* score of 0.137). Visual inspection reveals an obvious mechanism for escaping inhibition by TMP. A Trp residue at position 28 replaces a typically found Leu, and its bulk sterically occludes the substrate binding site specifically at the trimethoxyphenyl ring of TMP (Figure S1 of the Supporting Information). The structure of dihydrofolate is based on a dihydropterin heterocycle linked to a central benzoyl by a methylamino group. While the Trp residue does closely approach the portion of the folate substrate containing the methylamino linkage, minimal alterations in the protein geometry are able to relieve the clash. In so doing, the Trp side chain fits well with the face of the central benzoyl moiety. In contrast, TMP and related scaffolds link a single aromatic pyrimidine ring to a central benzoyl moiety by a methyl group, providing much shorter spacing and resulting in a direct clash between the mutated Trp side chain and the inhibitor. To overcome this resistant mechanism, a scaffold different from that of TMP will be required.

■ CONCLUSIONS

The goals of this work were to characterize the DHFR enzyme from *E. faecalis*, to determine the capacity of the dihydrophthalazine series to inhibit this enzyme, and to derive preferences in inhibitor structure. Early work to clarify treatment modalities for *E. faecalis* revealed a reversal of anti-folate inhibition if a metabolically active product analogue of the folate pathway, folinic acid, was included in the medium.[14] Continuing studies sought to address the impact of those observations within an animal model of peritoneal infection and documented an inferior outcome with TMP-SMX treatment.[17] However, peritoneal spaces have a demonstrated capacity to serve as reservoirs for folate metabolites, so this result is not surprising.[45] Our investigations were able to only marginally reproduce this effect for *E. faecalis*, limited to an increase in the MIC of one dilution or less for TMP or for the anti-folate series under investigation. Interestingly, the most striking increase in MIC was for the synergistic combination of TMP with SMZ. These results led us to surmise the possible existence of a strain-dependent acquired uptake mechanism that might not be present in the current strain, which is of great interest for further study. Larger increases in MIC values were noted for both *E. faecalis* and *S. aureus* under mildly acidic conditions, such as those found in urine. Overall, it is clear that the environment of the infection will play a crucial role in the efficacy of treatment with anti-folates or other classes of antimicrobials.

In general, the Ef DHFR binding site is able to form complexes with many modifications at the chiral center within the dihydrophthalazine heterocycle with a minimal impact on the overall efficacy. Inhibition of the enzyme displays some variation that correlates with the volume and shape of the modification. As noted in previous work with the DHFR enzyme from *S. aureus* or *B. anthracis*, a modification of three to four carbon lengths at this chiral center is preferred, as is an aromatic or more planar moiety such as OSU34 (phenyl) and OSU53 (isobutenyl).[19,20] Moreover, consistent with previous work is the presence of only the *S*-enantiomer of RAB-propyl in

the binding pocket despite the use of a racemic mixture in crystallization trials.[23] Interestingly, the OSU35 (trifluoropropyl) modification is more efficacious than the RAB-propyl inhibitor with the Ef DHFR. This is likely due to a unique polar subsite on Ef DHFR that, in the cocrystal structure with RAB-propyl, is seen to coordinate two ordered water molecules adjacent to the termini of the propyl moiety that form hydrogen bonds to residues His23 and Lys29 (Figure 2A). Finally, the presence of ordered water molecules buried within the substrate pocket leads us to conclude that the conserved pattern of hydrogen bonding between the DHFR protein and substrate or inhibitors is essentially preformed, with water molecules serving as placeholders in the "empty" pocket. These waters would thus seem to be important to the intrinsic structure of the protein and to the substrate binding site, and this arrangement is likely stabilized by neighboring waters previously identified as highly conserved but with unknown function.[46] This is also a reasonable mechanism for the recruitment and maintenance of water molecules important for hydride tunneling as required for catalysis.[47]

The presence of an alternate position for the dihydrophthalazine moiety was also found in structures with *S. aureus* DHFR complexed to RAB-propyl.[19] In these observations, the torsion was at the same location around the acryloyl linker, indicating this flexibility is an important determinant in the fit of the inhibitor, thereby allowing it to take advantage of any available subpockets of the binding site. While for *S. aureus* the subsite is a prominent surface feature, in the Ef DHFR this arrangement results from (1) a more shallow binding site at this position due to a bulkier Phe31 residue comprising the "floor", resulting in a somewhat higher position in the site for the phthalazine, and (2) a subpocket, smaller than that in *S. aureus*, that is created by movement of the binding site loop containing the insertion of cysteine at position 52. In general, the two dihydrophthalazine positions in Ef DHFR are spatially closer than those of *S. aureus*. Thus, while *S. aureus* DHFR is predicted to readily accommodate the *R*-enantiomer in the second position, Ef DHFR, like *B. anthracis* DHFR, seems to be capable of accepting only the *S*-enantiomer.

One of the effects of this insertion of Cys at a binding site loop is to generate a structure more like that of human DHFR, which has an inserted Pro-Glu-Lys-Asn sequence at a position equivalent to Cys52.[39] In the case of human DHFR, the "PEKN" insertion generates specificity by blocking access of the dihydrophthalazine to the binding site,[23] but in Ef DHFR, the effect on a single insertion is translated to the cofactor site. It is curious that among the three locations in the human DHFR enzyme that have been most altered in evolution, Ef DHFR shares changes at two of those, the Gly18 mutation and the Cys52 insertion, both of which contribute to altered NADPH docking.[39]

Although we are limited to only the two current structures for Ef DHFR, it is striking that the percentage of molecules with externally bound nicotinamide groups is increased from 60 to 80% in the presence of RAB-propyl. In the experimental procedure, NADPH was added during purification at least 3 days prior to saturation with RAB-propyl. As noted above, there are multiple courses that would result in the displaced nicotinamide, including reduced access due to the inserted Cys52 residue, oxidation of the cofactor, and/or general dynamics of enzymatic cycling. We now add to this the hypothesis that RAB-propyl plays a role in either blocking complete access to the binding pocket or displacing bound nicotinamide through steric mechanisms. This observation builds on our approach to use substrate mimics as competitive inhibitors that can have enhanced potency by perturbing cofactor dynamics.

The mutated DHFR enzyme encoded by *dfrF* has substantive changes in sequence that are expected to impact its global stability and cofactor interactions. We suggest that the *dfrF*-encoded enzyme is relatively unstable because of poor core packing of the protein. In contrast, the DHFR enzyme encoded by the *dfrK* gene appears to be likely to conform to known DHFR structural elements, and it contains amino acid substitutions that would block TMP and RAB-propyl inhibitor binding while likely maintaining interactions with the folate substrate needed for catalysis. At least one inhibitor class under development would overcome the predicted steric clash due to a novel propargyl linkage between a pyrimidine and a central benzoyl ring.[40] This arrangement more closely follows the shape of the natural dihydrofolate substrate and thus would not impinge on the substituted Trp residue (Figure S1 of the Supporting Information). A remaining question is the interplay of TMP^R enzymes with the hypothesized strain specific folate uptake machinery, which is of extreme interest for future investigations.

■ ASSOCIATED CONTENT

Ⓢ Supporting Information

A supplemental image of the comparison homology models for the TMP-resistant DHFR proteins encoded by the *dfrF* and *dfrK* genes. This material is available free of charge via the Internet at http://pubs.acs.org.

■ AUTHOR INFORMATION

Corresponding Author

*University of Oklahoma, 101 Stephenson Parkway, Norman, OK 73019. E-mail: cbourne@ou.edu. Phone: (405) 325-5348.

Present Addresses

[§]Department of Chemistry and Biochemistry, University of Oklahoma, Norman, OK 73019.

[∥]Department of Cell Biology, University of Oklahoma Health Sciences Center, Oklahoma City, OK 73104.

[⊥]Dow Chemical Co., Buffalo Grove, IL 60089.

Funding

This work was supported by funding from National Institute of Allergy and Infectious Diseases Grant R01-AI090685 to W.W.B.

Notes

The authors declare no competing financial interest.

■ ACKNOWLEDGMENTS

X-ray data were collected at the Macromolecular Crystallography Laboratory, University of Oklahoma, Norman, OK. DNA sequencing of clones and constructs was conducted at the Oklahoma State University Recombinant DNA and Protein Resource Facility. Figures were generated with the UCSF Chimera package, which is made freely available by the Resource for Biocomputing, Visualization, and Informatics and supported by National Institutes of Health Grant P41 RR-01081.

■ ABBREVIATIONS

DHFR, dihydrofolate reductase; TMP, trimethoprim; VRE, vancomycin-resistant *Enterococcus* (*faecalis*); SMZ, sulfame-

thoxazole; RAB-propyl, (*S*,*E*)-3-{5-[(2,4-diaminopyrimidin-5-yl)methyl]-2,3-dimethoxyphenyl}-1-[1-propylphthalazin-2(1*H*)-yl]-2-propen-1-one; NADPH, nicotinamide adenine dinucleotide phosphate; Ef, *E. faecalis*; MIC, minimal inhibitory concentration; IC_{50}, concentration producing 50% inhibition of a reaction; SEM, standard error of the mean; DTT, dithiothreitol; pABG, *p*-aminobenzoyl glutamate.

REFERENCES

(1) Hawser, S., Lociuro, S., and Islam, K. (2006) Dihydrofolate reductase inhibitors as antibacterial agents. *Biochem. Pharmacol. 71*, 941−948.

(2) Bowden, K., Harris, N. V., and Watson, C. A. (1993) Structure-activity relationships of dihydrofolate reductase inhibitors. *J. Chemother. 5*, 377−388.

(3) Molina, J. R. (2008) Pralatrexate, a dihydrofolate reductase inhibitor for the potential treatment of several malignancies. *IDrugs 11*, 508−521.

(4) Coque, T. M., Singh, K. V., Weinstock, G. M., and Murray, B. E. (1999) Characterization of dihydrofolate reductase genes from trimethoprim-susceptible and trimethoprim-resistant strains of *Enterococcus faecalis*. *Antimicrob. Agents Chemother. 43*, 141−147.

(5) Lopez, M., Kadlec, K., Schwarz, S., and Torres, C. (2012) First detection of the *Staphylococcal* trimethoprim resistance gene *dfrK* and the *dfrK*-carrying transposon Tn559 in *Enterococci*. *Microb. Drug Resist. 18*, 13−18.

(6) Kadlec, K., and Schwarz, S. (2009) Identification of a novel trimethoprim resistance gene, *dfrK*, in a methicillin-resistant *Staphylococcus aureus* ST398 strain and its physical linkage to the tetracycline resistance gene tet(L). *Antimicrob. Agents Chemother. 53*, 776−778.

(7) Beierlein, J. M., Karri, N. G., and Anderson, A. C. (2010) Targeted mutations of *Bacillus anthracis* dihydrofolate reductase condense complex structure-activity relationships. *J. Med. Chem. 53*, 7327−7336.

(8) Dale, G. E., Broger, D., D'Arcy, A., Hartman, P. G., DeHoogt, R., Jolidon, S., Kompis, I., Labhardt, A. M., Langen, H., Locher, H., Page, M. G., Stüber, D., Then, R. L., Wipf, B., and Oefner, C. (1997) A single amino acid substitution in *Staphylococcus aureus* dihydrofolate reductase determines trimethoprim resistance. *J. Mol. Biol. 266*, 23−30.

(9) Dale, G. E., Langen, H., Page, M. G. P., Then, R. L., and Stüber, D. (1995) Cloning and characterization of a novel, plasmid-encoded trimethoprim-resistant dihydrofolate reductase from *Staphylococcus haemolyticus* MUR313. *Antimicrob. Agents Chemother. 39*, 1920−1924.

(10) Silver, L. L. (2011) Challenges of antibacterial discovery. *Clin. Microbiol. Rev. 24*, 71−109.

(11) Hollenbeck, B. L., and Rice, L. B. (2012) Intrinsic and acquired resistance mechanisms in *Enterococcus*. *Virulence 3*, 421−433.

(12) Paulsen, I. T., Banerjei, L., Myers, G. S., Nelson, K. E., Seshadri, R., Read, T. D., Fouts, D. E., Eisen, J. A., Gill, S. R., Heidelberg, J. F., Tettelin, H., Dodson, R. J., Umayam, L., Brinkac, L., Beanan, M., Daugherty, S., DeBoy, R. T., Durkin, S., Kolonay, J., Madupu, R., Nelson, W., Vamathevan, J., Tran, B., Upton, J., Hansen, T., Shetty, J., Khouri, H., Utterback, T., Radune, D., Ketchum, K. A., Dougherty, B. A., and Fraser, C. M. (2003) Role of mobile DNA in the evolution of vancomycin-resistant *Enterococcus faecalis*. *Science 299*, 2071−2074.

(13) Eliopoulos, G. M. (2009) Microbiology of drugs for treating multiply drug-resistant Gram-positive bacteria. *J. Infect. 59* (Suppl. 1), S17−S24.

(14) Zervos, M. J., and Schaberg, D. R. (1985) Reversal of the *in vitro* susceptibility of *Enterococci* to trimethoprim-sulfamethoxazole by folinic acid. *Antimicrob. Agents Chemother. 28*, 446−448.

(15) de Crecy-Lagard, V., El Yacoubi, B., de la Garza, R. D., Noiriel, A., and Hanson, A. D. (2007) Comparative genomics of bacterial and plant folate synthesis and salvage: Predictions and validations. *BMC Genomics 8*, 245.

(16) Fulyani, F., Schuurman-Wolters, G. K., Zagar, A. V., Guskov, A., Slotboom, D. J., and Poolman, B. (2013) Functional diversity of tandem substrate-binding domains in ABC transporters from pathogenic bacteria. *Structure 21*, 1879−1888.

(17) Chenoweth, C. E., Robinson, K. A., and Schaberg, D. R. (1990) Efficacy of ampicillin versus trimethoprim-sulfamethoxazole in a mouse model of lethal *Enterococcal* peritonitis. *Antimicrob. Agents Chemother. 34*, 1800−1802.

(18) Wisell, K. T., Kahlmeter, G., and Giske, C. G. (2008) Trimethoprim and *Enterococci* in urinary tract infections: New perspectives on an old issue. *J. Antimicrob. Chemother. 62*, 35−40.

(19) Bourne, C. R., Barrow, E. W., Bunce, R. A., Bourne, P. C., Berlin, K. D., and Barrow, W. W. (2010) Inhibition of antibiotic-resistant *Staphylococcus aureus* by the broad-spectrum dihydrofolate reductase inhibitor RAB1. *Antimicrob. Agents Chemother. 54*, 3825−3833.

(20) Bourne, C. R., Wakeham, N., Nammalwar, B., Tseitin, V., Bourne, P. C., Barrow, E. W., Mylvaganam, S., Ramnarayan, K., Bunce, R. A., Berlin, K. D., and Barrow, W. W. (2013) Structure-activity relationship for enantiomers of potent inhibitors of *B. anthracis* dihydrofolate reductase. *Biochim. Biophys. Acta 1834*, 46−52.

(21) Barrow, E. W., Dreier, J., Reinelt, S., Bourne, P. C., and Barrow, W. W. (2007) *In vitro* efficacy of new anti-folates against trimethoprim-resistant *Bacillus anthracis*. *Antimicrob. Agents Chemother. 51*, 4447−4452.

(22) Caspers, P., Bury, L., Gaucher, B., Heim, J., Shapiro, S., Siegrist, S., Schmitt-Hoffmann, A., Thenoz, L., and Urwyler, H. (2009) *In vitro* and *in vivo* properties of dihydrophthalazine anti-folates, a novel family of antibacterial drugs. *Antimicrob. Agents Chemother. 53*, 3620−3627.

(23) Bourne, C. R., Bunce, R. A., Bourne, P. C., Berlin, K. D., Barrow, E. W., and Barrow, W. W. (2009) Crystal structure of *Bacillus anthracis* dihydrofolate reductase with the dihydrophthalazine-based trimethoprim derivative RAB1 provides a structural explanation of potency and selectivity. *Antimicrob. Agents Chemother. 53*, 3065−3073.

(24) Nammalwar, B., Bunce, R. A., Berlin, K. D., Bourne, C. R., Bourne, P. C., Barrow, E. W., and Barrow, W. W. (2012) Synthesis and biological activity of substituted 2,4-diaminopyrimidines that inhibit *Bacillus anthracis*. *Eur. J. Med. Chem. 54*, 387−396.

(25) *Methods for dilution antimicrobial susceptibility tests for bacteria that grow aerobically*, approved standard 8th ed. (2009) Vol. *29*, pp 1−65, Clinical and Laboratory Standards Institute, Wayne, PA.

(26) *KC Jr.* (2010) BioTek, Winooski, VT.

(27) Cheng, Y., and Prusoff, W. H. (1973) Relationship between the inhibition constant (Ki) and the concentration of inhibitor which causes 50% inhibition (I50) of an enzymatic reaction. *Biochem. Pharmacol. 22*, 3099−3108.

(28) Battye, T. G., Kontogiannis, L., Johnson, O., Powell, H. R., and Leslie, A. G. (2011) iMOSFLM: A new graphical interface for diffraction-image processing with MOSFLM. *Acta Crystallogr. D67*, 271−281.

(29) Evans, P. (2006) Scaling and assessment of data quality. *Acta Crystallogr. D62*, 72−82.

(30) McCoy, A. J., Grosse-Kunstleve, R. W., Adams, P. D., Winn, M. D., Storoni, L. C., and Read, R. J. (2007) Phaser crystallographic software. *J. Appl. Crystallogr. 40*, 658−674.

(31) Adams, P. D., Afonine, P. V., Bunkoczi, G., Chen, V. B., Davis, I. W., Echols, N., Headd, J. J., Hung, L. W., Kapral, G. J., Grosse-Kunstleve, R. W., McCoy, A. J., Moriarty, N. W., Oeffner, R., Read, R. J., Richardson, D. C., Richardson, J. S., Terwilliger, T. C., and Zwart, P. H. (2010) PHENIX: A comprehensive Python-based system for macromolecular structure solution. *Acta Crystallogr. D66*, 213−221.

(32) Kim, H. S., Damo, S. M., Lee, S. Y., Wemmer, D., and Klinman, J. P. (2005) Structure and hydride transfer mechanism of a moderate thermophilic dihydrofolate reductase from *Bacillus stearothermophilus* and comparison to its mesophilic and hyperthermophilic homologues. *Biochemistry 44*, 11428−11439.

(33) Emsley, P., and Cowtan, K. (2004) Coot: Model-building tools for molecular graphics. *Acta Crystallogr. D60*, 2126−2132.

(34) Sobolev, V., Sorokine, A., Prilusky, J., Abola, E. E., and Edelman, M. (1999) Automated analysis of interatomic contacts in proteins. *Bioinformatics 15*, 327−332.

(35) Laskowski, R. A., and Swindells, M. B. (2011) LigPlot+: Multiple ligand-protein interaction diagrams for drug discovery. *J. Chem. Inf. Model. 51*, 2778−2786.
(36) Arnold, K., Bordoli, L., Kopp, J., and Schwede, T. (2006) The SWISS-MODEL workspace: A web-based environment for protein structure homology modelling. *Bioinformatics 22*, 195−201.
(37) Anderson, A. C., Beierlein, J. M., Viswanathan, K., and Wright, D. L. (2014) Structure-activity studies of heterocyclic propargyl-lined TMP analogs targeting *Bacillus anthracis* dihydrofolate reductase. Manuscript to be submitted for publication.
(38) Sawaya, M. R., and Kraut, J. (1997) Loop and subdomain movements in the mechanism of *Escherichia coli* dihydrofolate reductase: Crystallographic evidence. *Biochemistry 36*, 586−603.
(39) Liu, C. T., Hanoian, P., French, J. B., Pringle, T. H., Hammes-Schiffer, S., and Benkovic, S. J. (2013) Functional significance of evolving protein sequence in dihydrofolate reductase from bacteria to humans. *Proc. Natl. Acad. Sci. U.S.A. 110*, 10159−10164.
(40) Wright, D. L., and Anderson, A. C. (2011) Anti-folate agents: A patent review (2006−2010). *Expert Opin. Ther. Pat. 21*, 1293−1308.
(41) Whitlow, M., Howard, A. J., Stewart, D., Hardman, K. D., Chan, J. H., Baccanari, D. P., Tansik, R. L., Hong, J. S., and Kuyper, L. F. (2001) X-ray crystal structures of *Candida albicans* dihydrofolate reductase: High resolution ternary complexes in which the dihydronicotinamide moiety of NADPH is displaced by an inhibitor. *J. Med. Chem. 44*, 2928−2932.
(42) Meijers, R., and Cedergren-Zeppezauer, E. (2009) A variety of electrostatic interactions and adducts can activate NAD(P) cofactors for hydride transfer. *Chem.-Biol. Interact. 178*, 24−28.
(43) Rost, B. (1999) Twilight zone of protein sequence alignments. *Protein Eng. 12*, 85−94.
(44) Benkert, P., Biasini, M., and Schwede, T. (2011) Toward the estimation of the absolute quality of individual protein structure models. *Bioinformatics 27*, 343−350.
(45) Bunni, M. A., Sirotnak, F. M., Otter, G. M., and Priest, D. G. (1994) Disposition of leucovorin and its metabolites in the plasma, intestinal epithelium, and intraperitoneal L1210 cells of methotrexate-pretreated mice. *Cancer Chemother. Pharmacol. 34*, 455−458.
(46) Nammalwar, B., Bourne, C. R., Bunce, R. A., Wakeham, N., Bourne, P. C., Ramnarayan, K., Mylvaganam, S., Berlin, K. D., Barrow, E. W., and Barrow, W. W. (2012) Inhibition of Bacterial Dihydrofolate Reductase by 6-Alkyl-2,4-diaminopyrimidines. *ChemMedChem 7*, 1974−1982.
(47) Stojkovic, V., Perissinotti, L. L., Willmer, D., Benkovic, S. J., and Kohen, A. (2012) Effects of the donor-acceptor distance and dynamics on hydride tunneling in the dihydrofolate reductase catalyzed reaction. *J. Am. Chem. Soc. 134*, 1738−1745.